DOI: 10.1002/ejic.200600418

Modelling the Electron-Transfer Complex Between Aldehyde Oxidoreductase and Flavodoxin

Ludwig Krippahl,[a] P. Nuno Palma,[a][‡] Isabel Moura,[a] and José J. G. Moura*[b]

Keywords: Bioinorganic chemistry / Electron transfer / Molybdenum / Enzyme models

Three-dimensional protein structures of the xanthine oxidase family show different solutions for the problem of transferring electrons between the flavin adenine dinucleotide (FAD) group and the molybdenum cofactor. In xanthine oxidase all the cofactors lie within domains of the same protein chain, whereas in CO dehydrogenase the Fe–S centres, FAD and Mo cofactors are enclosed in separate chains and the enzyme exists as a stable complex of all three. In aldehyde oxidoreductase, only Fe–S and Mo co-factors are present in a single protein chain. Flavodoxin is docked to aldehyde oxidoreductase to mimic the flavin component on the intramolecular electron transfer chain of aanthine oxidase and CO dehydrogenase and, remarkably, the main features of the electron-transfer pathway are observed.

Introduction

Molybdenum and tungsten are found in a mononuclear form in the active site of a diverse group of enzymes that catalyze, in general, oxygen-atom transfer and are distinct from the nitrogenase enzyme that contains a complex FeSMo cluster. Mononuclear Mo-enzymes have been classified into three main groups, called the xanthine oxidase (XO), dimethyl sulfoxide reductase (DMSOR) and sulfite oxidase (SO) families.[1,2] The active site of these enzymes contains the metal atom coordinated to one or two pyranopterin molecules and to a variable number of ligands containing atoms such as oxygen (oxo, hydroxo, water, serine, and aspartic acid), sulfur (cysteines) and selenium (selenocysteines). Pyranopterin is an organic ligand that can be either in the monophosphate form or have a nucleotide molecule attached by a pyrophosphate link. In addition, these proteins may have other redox cofactors such as iron-sulfur (Fe–S) centres, hemes and flavin groups, which are involved in intra- and intermolecular electron-transfer processes.[1–3]

There are a few known crystal structures of molybdenum hydroxylases from the XO family. These include aldehyde oxidoreductase (AOR) from *Desulfovibrio gigas*,[4–6] xanthine oxidoreductase (XO) from *Bos taurus*[7] and Xanthine dehydrogenase (XDH) from *Rhodobacter capsulatus*.[8] There are also two known crystal structures of similar proteins containing Mo, namely CO dehydrogenase (CODH) from *Oligotropha carboxidovorans*, which catalyzes the oxidation of CO to CO_2 without cleavage of a C–H bond,[9,10] and 4-hydroxybenzoyl-CoA Reductase (4-HBCR) from *Thaurea aromatica*, which catalyzes reductive removal of an aromatic hydroxy group.[11,12]

Despite their similarity, these proteins show three different sequence arrangements for the active sites participating in electron transfer between the FAD group: the two [2Fe-2S] centres and the Molybdenum cofactor.[1,2,7–14] In general, all the cofactors in XO and XDH lie within domains of the same protein chain, although some exceptions are found in prokaryotic XDHs such as the one isolated from *Rhodobacter capasulatus.* In CODH and 4-HBCR, two [2Fe-2S] centres, one FAD and one Mo cofactor are enclosed in separate chains and the enzyme exists as a stable complex of all three. In AOR only the two [2Fe-2S] centres and Mo cofactor are present in a single and shorter polypeptide chain (Figure 1).

Although the arrangement of the 4-HBCR subunits containing the FAD group, the molybdenum cofactor and the two intermediary [2Fe-2S] centres is similar to that of CODH, 4-HBCR is significantly different from CODH. The gene sequences for the three subunits of 4-HBCR in *Rhodopseudomonas palustris*[15] and *T. aromatica*[13] reveal significant differences between these proteins, and 4-HBCR consists of three subunits of $(\alpha\beta\gamma)_2$ composition.[16,17] Each monomer contains a [4Fe-4S] centre[16] in addition to the prosthetic groups shared with CODH. The additional [4Fe-4S] centre is coordinated to conserved cysteinyl residues in a unique stretch of approximately 40 amino acids in the β subunit.[12,19] Nevertheless, for the purposes of this work the important features of 4-HBCR are shared with CODH,

[a] REQUIMTE-CQFB, Departamento de Química, Faculdade de Ciências e Tecnologia, Universidade Nova de Lisboa, 2829-516 Campus de Caparica, Portugal
[b] REQUIMTE-CQFB, Departamento de Química, Faculdade de Ciências e Tecnologia, Universidade Nova de Lisboa, 2829-516 Campus de Caparica, Portugal
Fax: +351-21-194-8550
E-mail: jose.moura@dq.fct.unl.pt
[‡] Present address: Laboratórios BIAL, Porto, Portugal

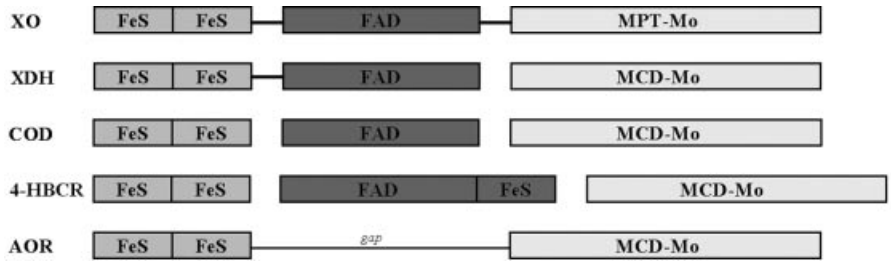

Figure 1. Schematic representation of the domain sequence for the three enzymes XO, CODH, 4-HBCR (that includes an extra elongation of the β-subunit that binds, in addition to the FAD moiety, the [4Fe-4S] center) and AOR (homologies among molybdenum hydroxylases). The FAD domain is absent in the *D. gigas* aldehyde oxidoreductase. In the *R. capsulatus* Xanthine dehydrogenase and the *Bos Taurus* XO, the iron-sulphur and flavin-binding portions of the protein constitute one subunit (XdhA), and the molybdenum-binding portion a second (XdhB). In the *O. carboxydovorans* CO dehydrogenase, the iron–sulphur centres are together in one subunit (CoxS), the flavin in a second (CoxM) and the molybdenum in a third subunit (CoxL). A comparison with the *R. capsulatus* XDH domain sequence is also included (a variation of the XO domain theme).

namely the electron-transfer pathway involving the FAD, the two [2Fe-2S] centres and the Mo cofactor.

The molybdenum [iron-sulfur] protein, first isolated from *Desulfovibrio gigas* (*Dg*AOR),[18] was later shown to mediate the electronic flow from salicylaldehyde to a suitable electron acceptor, and its 2,6-dichlorophenolindophenol (DCPIP)-dependent aldehyde oxidoreductase activity was studied in detail[19] using a wide range of aldehydes and analogues. A steady-state kinetic analysis (K_M and V_{max}) was performed for acetaldehyde, propionaldehyde, benzaldehyde and salicylaldehyde in the presence of a suitable electron acceptor (DCPIP), and a simple Michaelis–Menten model was shown to be applicable as a first kinetic approach. Xanthine, purine, allopurinol and *N*1-methylnicotinamide (NMN), however, could not be utilized as enzyme substrates. DCPIP and ferricyanide were shown to be capable of cycling the electronic flow, whereas other cation and anion dyes [O_2 and $NAD(P)^+$] were not active in this process. This molybdenum hydroxylase was later shown to be part of an electron-transfer chain that is capable of linking the oxidation of aldehydes to the reduction of protons and involves flavodoxin.[20]

The FAD domain, which is present in XO and CODH but absent in AOR, and the evidence for in vitro electron transfer between AOR and flavodoxin, led to the reasonable assumption that flavodoxin can play the role of a reaction partner for AOR that replaces the missing domain. Our hypothesis was that the interaction between AOR and flavodoxin should mimic the arrangement of the domains or subunits of the other similar proteins, therefore to test this hypothesis we attempted to model the AOR-flavodoxin complex using the BiGGER docking algorithm.[21,22]

Results and Discussion

Our hypothesis was thus that if flavodoxin assumed the role of the missing FAD domain, the complex of flavodoxin with AOR should be similar to the structures of CODH and XO, and should be consistent with the experimental data available.[20]

The Nature of the Electron-Transfer Complex

The interaction between AOR and flavodoxin seems to be driven mostly by electrostatics, since both partners are highly charged and flavodoxins have high dipolar moments (approx. 400 Debye). Both AOR and flavodoxin are acidic, but the reaction rate of electron transfer, as measured using aldehydes as electron donor through AOR and following the formation of flavodoxin semiquinone state at 590 nm (Figure 2) (experimental conditions as in ref.[20]; see also caption to Figure 2), increased with increasing ionic strength up to 0.1 M. Although the strong ionic-strength dependency of the reaction kinetics for the electron transfer between AOR and flavodoxin from *D. gigas* indicates that the interaction is driven mostly by electrostatics, it was intriguing that the reaction rate increased with increasing ionic strength. However, the docking results (see below) helped to explain this observation and called our attention to the effect of ionic strength on the electrostatic field generated

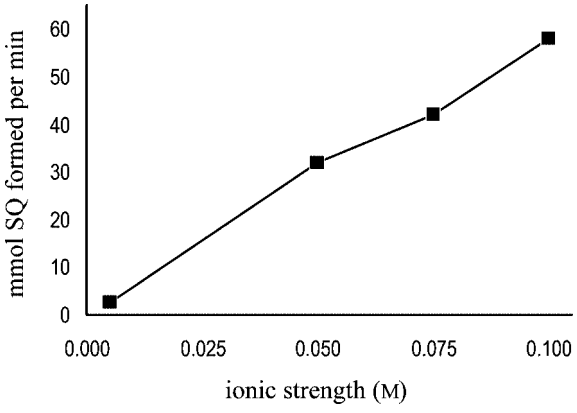

Figure 2. Dependency of the AOR-flavodoxin reaction rate on ionic strength. The reaction rate was measured by the formation of the semiquinone form of FAD, which was followed by spectroscopy at 590 nm. Anaerobic formation of flavodoxin semiquinone was followed at 580 nm, using benzaldehyde as electron donor, varying the media ionic strength (adjusted with NaCl). The experiments were conducted at 20 °C and pH 7.6 (Tris-HCl buffer). AOR was 2 μM, flavodoxin 24 μM and substrate 100 μM. General procedures as detailed indicated in ref.[20]

by AOR at the suggested interaction site, near the more exposed [2Fe-2S] moiety. Figure 3 shows the electrostatic field in this region at an ionic strength of 0.0, 0.1 and 0.5 M. The electrostatic field was calculated by solving the linearised Poisson–Boltzmann equation with a multi-grid finite difference solver,[23] with a grid resolution of 2 Å. The simplifying assumptions (equal concentrations and radii for positive and negative ions and linearisation of the hyperbolic sine term) and the finite difference solution limit the precision of the calculations, but this is not important for the qualitative result that explains the effects of ionic strength on this reaction. At higher ionic strength the overall negative charge of AOR has less influence near the positive patch surrounding the exposed [2Fe-2S] cluster, thus allowing a positive region of the field to project farther from the surface and possibly helping to guide the negatively charged flavodoxin. This explains both the reaction kinetics data and how these two strongly acidic proteins may interact despite their large negative charge.

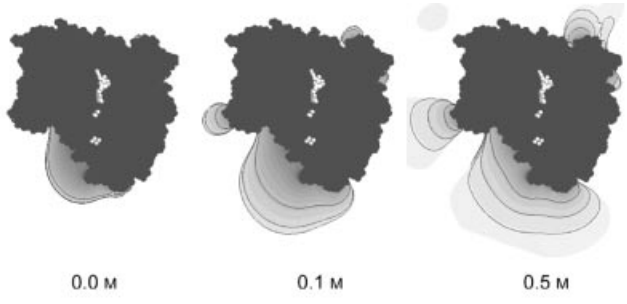

Figure 3. The three panels show the positive regions of the electrostatic field projected by AOR at 0.0, 0.1 and 0.5 M of ionic strength. The isopotential lines are for 0.1, 0.01 and 0.001 kcal mol. Only the positive regions of the electrostatic field are shown. The more exposed [2Fe-2S] cluster is shown on the lower part of each panel, and the projecting positive region of the field corresponds to the most likely docking site (Figure 4).

AOR-Flavodoxin Complex: Docking Model

We used the BiGGER[21,22] docking algorithm both with the default soft docking parameters and with the hard docking option for all docking runs. The first stage of the docking algorithm was to select a set of 5000 solutions from all possible configurations and generate candidate complexes by shifting one of the partners relative to the other in steps of 1 Å of translation for each 15°-step in rotation. This exhaustive search generated billions of possibilities, most of which were excluded by eliminating excessive overlap and by keeping only those with the highest surface contact areas.

The soft docking algorithm[22] is a general docking algorithm applicable to cases ranging from tightly binding enzyme-inhibitor complexes to transient electron-transfer interactions, and so must take into account the effects of side-chain flexibility, which is potentially essential in strong interactions. This algorithm models side-chain flexibility implicitly by allowing some interatomic clashes involving selected regions of flexible side-chains at the surface of the protein. The downside is an increase in the fraction of incorrect models retained in those cases where side-chain flexibility is not a relevant factor. In such cases, which are common for weak interactions, the hard docking alternative tends to provide clearer results. Our approach was to use both alternatives to take advantage of the best features of each. Agreement between hard docking and soft docking results indicated that it was not necessary to account for side-chain conformation changes. In such cases we can use the hard docking results, which are generally clearer and easier to interpret. If the results of the two alternatives disagree, then we should use the soft docking models because this suggests side-chain conformation changes may be an important factor in the formation of the complex. In the case of the AOR-flavodoxin complex studied here, the results of hard docking agreed with those of soft docking − both approaches gave similar clusters of models among the highest ranking − so all results presented here are for hard docking. This agreement of the six different docking simulations, with different conditions and partners, shows the simulations to be reliable. Furthermore, in all cases there are structures with the configuration predicted by our hypothesis among the highest scoring models when ranked by the electrostatic interaction score.

The second stage of BiGGER is the ranking stage, in which the 5000 models are evaluated according to electrostatics, solvent exclusion, and surface complementarity and amino acid contacts. The global scoring function included in BiGGER is also designed for general applicability by combining these different factors to give a single score optimised to separate correct models from incorrect models over a broad range of complexes. This is the best option when no information is available regarding the interaction being studied. However, BiGGER also provides the hydrophobicity and electrostatic scores for those cases in which it is possible to estimate if the interaction is driven mainly by solvation effects or by electrostatics.[21,22] Since this was one such case, we chose to use the electrostatic score to rank the most likely models. Nevertheless, the global score also placed high scoring models in the same region (including the highest ranking model).

The choice of the electrostatic interaction score was dictated by experimental data on the ionic-strength dependency of the electron-transfer reaction between flavodoxin and AOR (both form *D. gigas*), and by the large charge of the partners, which suggested electrostatics to be the main driving force in this interaction. Furthermore, the docking simulations also suggested that the interaction between AOR and flavodoxin is strongly driven by electrostatics, since the electrostatic score value was high, with an estimated enthalpy for the electrostatic interaction of approximately 100 kcal mol^{-1}. This is an approximate value due to the fact that it is calculated from a simple Coulombic model and the docking models generated by BiGGER are not very precise as the translation search is in steps of 1 Å and the side-chain placement was not optimised for each model. However, these simplified calculations are the only practical

way of dealing with thousands of candidate models without excessive computational demands, and the results do not require precise energy estimates, as all six simulations were in agreement and the estimated energy contributed by electrostatics was one to two orders of magnitude greater than that for hydrophobicity. Overall, all the simulation results and experimental data agree that the interaction between these proteins is essentially due to electrostatics.

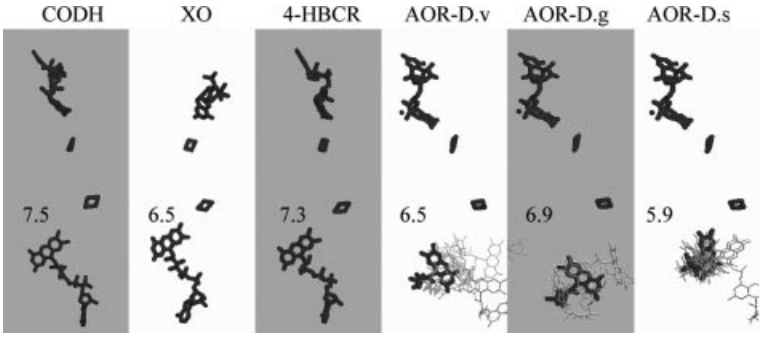

Figure 4. The relative positions of the FAD prosthetic groups for COD, XO, and 4-HBCR (first three panels) and the best models for the AOR-flavodoxin complex using the *D. vulgaris*, *D. gigas* and *D. salexigens* flavodoxins (last three panels). For the docking models the highest ranking configuration is shown in thick lines, and other high ranking configurations in thin lines. The numbers indicate the distances (in Å) between the cofactors. For the AOR-flavodixin complexes, the smallest distance of the fifteen highest ranking models is shown.

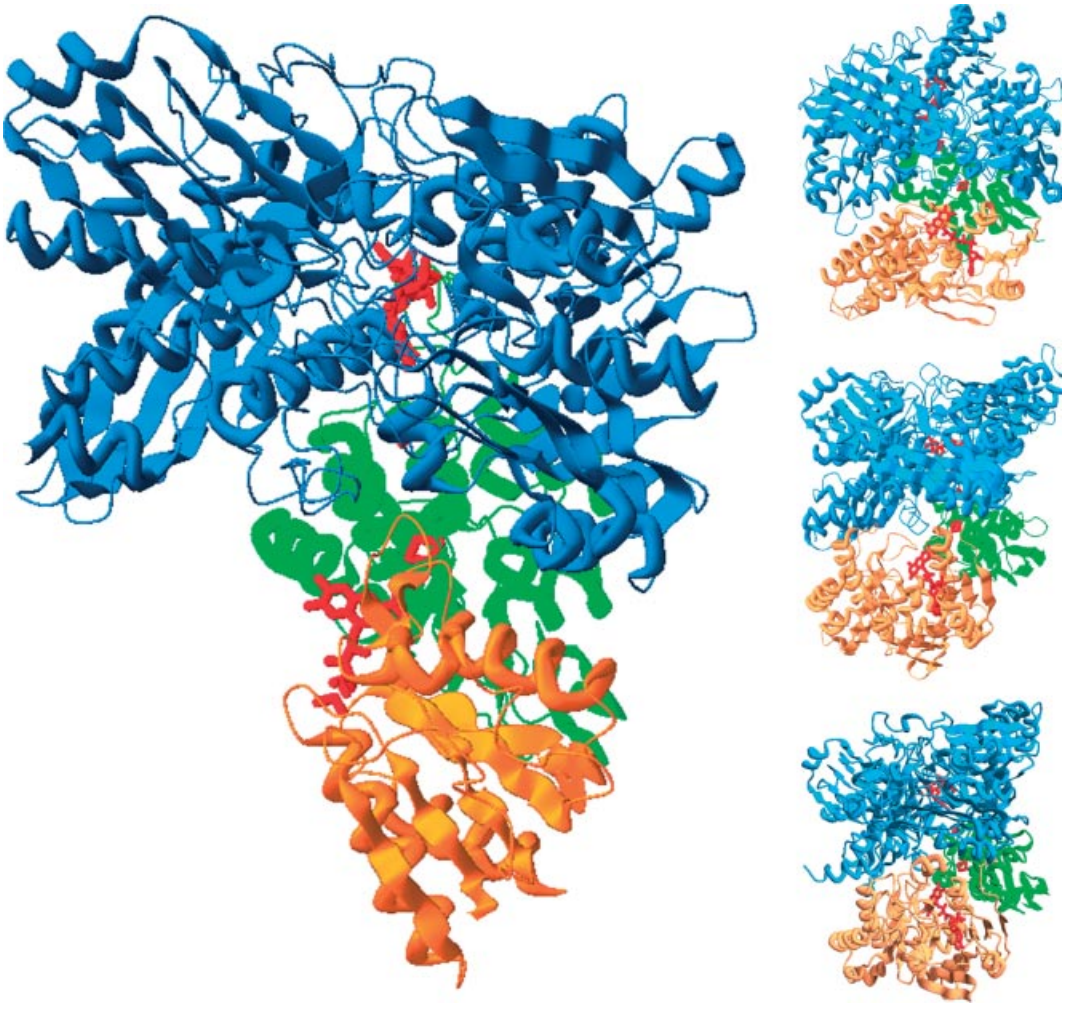

Figure 5. One possible docking configuration for *D. gigas* flavodoxin and AOR (left panel) compared with the structures of XO (top right), COD (centre right) and 4-HBCR (bottom right). The colours correspond to the sequence homology schemes shown in Figure 1, green for the FeS regions, orange for the FAD and flavodoxin, and blue for the MCD-Mo or MPT-Mo regions.

In short, all the docking results presented are for hard docking with electrostatic scoring. To model the complex between the flavodoxin and aldehyde oxidoreductase (AOR) from *Desulfovibrio gigas* we used the following structures:

– the X-ray structure for AOR (PDB code 1hlr, after correcting the transformation matrix to generate the dimer),[4,6]

– a homology model for the *D. gigas* flavodoxin using the Swiss-PROT sequence Q01095[24] and the structure from the *D. vulgaris* flavodoxin (PDB code 1fx1),[25]

– a homology model for the *D. salexigens* flavodoxin based on the *D. vulgaris* flavodoxin structure 1fx1,

– the *D. vulgaris* flavodoxin structure 1fx1.

Our goal was to model the *D. gigas* complex, although flavodoxins from *D. vulgaris* and *D. salexigens* also form productive complexes in vitro (unpublished data). Since the structure for the *D. gigas* flavodoxin was a model generated by homology, the other two − one a crystallographic structure and the other also a homology model − could be used to check the consistency of the results and verify that the *D. gigas* flavodoxin model was appropriate for our purposes. This was indeed the case, with the docking results for *D. salexigens* and *D. vulgaris* flavodoxin complexes being virtually identical to those obtained for the *D. gigas* flavodoxin.

We cannot give one unique model for the MOP-flavodoxin complex, and the interaction is most likely dynamic and cannot be represented by a single structure. However, these results indicate that flavodoxin interacts by docking near the exposed Fe–S cluster in a configuration resembling the structures of Xanthine oxidase (Figures 4 and 5). The distances between the FAD and [2Fe-2S] groups are similar in all three cases, with the shortest distance in the fifteen highest ranking models ranging between 6 and 7 Å, values similar to those of CODH, XO and 4-HBCR. Although not evident from the figure, in the models with the shortest distances among the highest ranking the dimethylbenzene part of the isoalloxazine ring is pointing towards the [2Fe-2S] centre in a manner analogous to CODH, XO and 4-HBCR. Despite this structural similarity, the contact surface of the flavodoxin in the AOR-flavodoxin models is less than half the contact surface of the FAD domain in XO. The contact surface area for flavodoxin, calculated with the DSSP program,[26] was no higher than 930 Å^2 (value for the model with largest surface contact among the highest ranking models), whereas the contact surface for the corresponding domain in XO is 2250 Å^2. This may explain why the XO complex is stable while AOR-flavodoxin is a transient complex.

Conclusions

AOR was previously shown to be part of an electron-transfer chain comprising four different soluble proteins from *D. gigas*, namely:

AOR → flavodoxin → Cyt c_3 (4 hemes) → (NiFe) Hydrogenase

comprising a total of 11 discrete redox centres, which is capable of linking the oxidation of aldehydes to the reduction of protons to hydrogen and involves a flavodoxin-FMN semiquinone state.[22] The intramolecular electron-transfer process within AOR will follow, in the presence of substrate, the electron flow from Mo to the proximal [2Fe-2S] centre and then to the distal [2Fe-2S] centre and the redox partner, modelled here as flavodoxin.

Molybdenum hydroxylases (XO family) are a remarkable example of how biology finds a wide range of structural solutions to build up a required electron-transfer array of redox centres. Different arrangements of the building blocks (protein chains and domains) give rise to similar 3D placements of the redox cofactors participating in this optimised ET reaction. The docking results for the AOR-flavodoxin complex support the hypothesis of structural and functional equivalence to the active-site arrangements found in CODH and XO, and the smaller contact surface suggests an explanation for the AOR-flavodoxin complex being less stable than the otherwise similar XO.

This modular construction of complex enzymes by rearrangement of sub-domains and sub-units is a general observation. Superoxide reductases are also a good example,[27,28] but not unique. Relatively exposed sub-domains with characteristic structures that are recognized in simple electron-transfer proteins are, in most cases, used as docking sites for electron-transfer partners (i.e. ferredoxin folding in hydrogenase,[29] plant-type ferredoxin folding in AOR (see ref.[4] and this work) and Fd-NADPH reductase[30]).

A more complex situation was found for the structural homologue 4-HBCR,[12] which contains an additional iron-sulfur centre, whereby a low-potential ferredoxin serves as in vivo electron donor for the enzyme.[11,16] The redox potentials of the FAD$^{\cdot}$/FADH and $Mo^{V/IV}$ transitions are exceptionally low, thus making 4-HBCR the only member of the XO family whose function is to catalyze the reduction of the substrate and suggesting an inverted electron flow. But, even so, a conserved architecture is also maintained for the three key redox sites (Mo, 2 [2Fe-2S] centres and FAD).

Acknowledgments

This work was supported by FCT-MCTES and COST D21-WG006.

[1] R. Hille, *Chem. Rev.* **1996**, *96*, 2757.
[2] C. D. Brondino, M. J. Romão, I. Moura, J. J. G. Moura, *Curr. Opin. Biol. Chem*. **2006**, in press.
[3] M. K. Johnson, D. C. Rees, M. W. Adams, *Chem. Rev.* **1996**, *96*, 2817.
[4] M. J. Romão, M. Archer, J. J. G. Moura, I. Moura, J. LeGall, R. Engh, M. Schneider, P. Hof, R. O. Duarte, R. Huber, *Science* **1995**, *270*, 1170.
[5] R. Huber, P. Hof, R. O. Duarte, J. J. G. Moura, I. Moura, M.-Y. Liu, J. LeGall, R. Hille, M. Archer, M. J. Romão, *Proc. Natl. Acad. Sci. USA* **1996**, *93*, 8846.
[6] J. M. Rebelo, J. M. Dias, R. Huber, J. J. G. Moura, M. J. Romão, *J. Biol. Inorg. Chem.* **2001**, *6*, 791.

[7] C. Enroth, B. T. Eger, K. Okamoto, T. Nishino, T. Nishino, E. F. Pai, *Proc. Natl. Acad. Sci. USA* **2000**, *97*, 10723.
[8] J. J. Truglio, K. Theis, S. Leimkühler, R. Rappa, K. V. Rajagopalan, C. Kisker, *Structure* **2002**, *10*, 115.
[9] H. Dobbek, L. Gremer, O. Meyer, R. Huber, *Proc. Natl. Acad. Sci. USA* **1999**, *96*, 8884.
[10] H. Dobbek, L. Gremer, L. Kiefersauer, R. Huber, O. Meyer, *Proc. Natl. Acad. Sci. USA* **1999**, *99*, 15971.
[11] K. Breese, G. Fuchs, *Eur. J. Biochem.* **1998**, *251*, 916.
[12] M. Unciuleac, E. Warkentin, C. C. Page, M. Boll, U. Ermler, *Structure* **2004**, *56*, 2249.
[13] R. Hille, *Arch. Biochem. Biophys.* **2005**, *433*, 107; R. Hille, *Eur. J. Inorg. Chem.* **2006**, 1913.
[14] K. Okamoto, K. Matsumoto, R. Hille, B. T. Eger, E. F. Pai, T. Nishino, *Proc. Natl. Acad. Sci. USA* **2004**, *101*, 793.
[15] J. Gibson, M. Dispensa, C. S. Harwood, *J. Bacteriol.* **1997**, *179*, 634.
[16] M. Boll, G. Fuchs, C. Meier, A. Trautwein, A. El Kasmi, S. W. Ragsdale, G. Buchanan, D. J. Lowe, *J. Biol. Chem.* **2001**, *276*, 47853.
[17] R. Brackmann, G. Fuchs, *Eur. J. Biochem.* **1993**, *213*, 563.
[18] J. J. G. Moura, A. V. Xavier, M. Bruschi, J. Le Gall, D. O. Hall, R. Cammack, *Biochem. Biophys. Res. Commun.* **1976**, *72*, 782.
[19] N. Turner, B. Barata, R. C. Bray, J. Deistung, J. LeGall, J. J. G. Moura, *Biochem. J.* **1987**, *243*, 755.
[20] B. A. Barata, J. LeGall, J. J. G. Moura, *Biochemistry* **1993**, *32*, 11559.
[21] P. N. Palma, L. Krippahl, J. E. Wampler, J. J. G. Moura, *Proteins: Struct., Function, Genetics* **2000**, *39*, 372.
[22] L. Krippahl, J. J. G. Moura, P. N. Palma, *Proteins: Struct., Funct., Genet.* **2003**, *52*, 19.
[23] I. Klapper, R. Hagstrom, R. Fine, K. Sharp, B. Honig, *Proteins* **1986**, *1*, 47.
[24] L. R. Helms, R. P. Swenson, *Biochim. Biophys. Acta* **1992**, *1131*, 325.
[25] K. D. Watenpaugh, L. C. Sieker, L. H. Jensen, J. Legall, M. Dubourdieu, *Proc. Natl. Acad. Sci. USA* **1972**, *69*, 3185.
[26] W. Kabsch, C. Sander, *Biopolymers* **1983**, *22*, 2577.
[27] C. Ascenso, F. Rusnak, I. Cabrito, M. J. Lima, S. Naylor, I. Moura, J. J. G. Moura, *J. Biol. Inorg. Chem.* **2000**, *5*, 720.
[28] T. Santos-Silva, J. Trincao, A. L. Carvalho, C. Bonifacio, F. Auchere, I. Moura, J. J. G. Moura, M. J. Romão, *Acta Crystallogr., Sect. F* **2005**, *61*, 967.
[29] X. Morelli, M. Czjzek, C. E. Hatchikian, O. Bornet, J. C. Fontecilla, P. N. Palma, J. J. G. Moura, F. Gurelesquin, *J. Biol. Chem.* **2000**, *275*, 23204.
[30] P. N. Palma, B. Lagoute, L. Krippahl, J. J. G. Moura, F. Guerlesquin, *FEBS Lett.* **2005**, *579*, 4585.

Received: May 7, 2006
Published Online: July 31, 2006

